Soft Matter

PAPER

View Article Online
View Journal | View Issue

Cite this: *Soft Matter*, 2023, **19**, 9399

Discontinuous rigidity transition associated with shear jamming in granular simulations†

Varghese Babu,*[a] H. A. Vinutha,[b] Dapeng Bi[c] and Srikanth Sastry*[a]

Received 3rd June 2023,
Accepted 27th September 2023

DOI: 10.1039/d3sm00725a

rsc.li/soft-matter-journal

We investigate the rigidity transition associated with shear jamming in frictionless, as well as frictional, disk packings in the quasi-static regime and at low shear rates. For frictionless disks, the transition under quasi-static shear is discontinuous, with an instantaneous emergence of a system spanning rigid clusters at the jamming transition. For frictional systems, the transition appears continuous for finite shear rates, but becomes sharper for lower shear rates. In the quasi-static limit, it is discontinuous as in the frictionless case. Thus, our results show that the rigidity transition associated with shear jamming is discontinuous, as demonstrated in the past for isotropic jamming of frictionless particles, and therefore a unifying feature of the jamming transition in general.

Granular materials can exist in a flowing or a solid state. The transition between these states, called the jamming transition, has been the subject of intense research,[1–3] particularly under isotropic compression of frictionless sphere packings. The jamming point ϕ_J for packings of soft particles exhibits many characteristics of a second-order phase transition, at which various quantities show power law scaling – with respect to the distance from the jamming point – as one compresses beyond the jamming point.[4,5] Furthermore, the distribution of small forces between particles just in contact, as well as the gaps between particles nearly in contact, also exhibits power law behavior. Exponents characterizing these are constrained by an inequality that is saturated for configurations at the jamming point, which are therefore "marginally stable".[6,7] The mean-field theory of glasses and jamming has predictions for these exponents which match numerical values for dimensions $D = 2$ and above.[5] Extensions of this theory predict these exponents to be the same for shear jamming, as recent numerical results indeed confirm, along with the aforementioned aspects of criticality.[8] These and related results[8,9] strongly support a unified description of both isotropic and shear jamming.

In contrast, the manner in which the contact network acquires rigidity is strongly discontinuous[10,11] for frictionless isotropic jamming. At the jamming point, the entire system (barring a small percentage of rattlers, described later) acquires rigidity discontinuously. From the Maxwell criterion for the rigidity of networks of nodes connected by edges representing distance constraints, the contact network of a configuration with N particles in D dimensions can be rigid when contacts result in at least $N_c = D(N - 1)$ constraints on the non-global degrees of freedom. In general, this is a necessary but not sufficient condition. Therefore, isotropic jamming occurs at the isostatic point, where the system has just the minimum number of contacts per particle, Z required, $Z_{iso} = 2D$ (from $\frac{NZ_{iso}}{2} = ND$). This discontinuous rigidity transition is different from the continuous transition observed, *e.g.* for sticky packings,[12,13] and in random spring networks[14,15] for which the rigid component of the system grows continuously beyond rigidity percolation, which does not occur at the isostatic point, and is preceded by the presence of both rigid and over-constrained regions.

Results available for shear jamming appear to suggest that the rigidity transition is continuous, in contrast to isotropic jamming.[16–19] Computational investigation of the rigidity transition for frictional two dimensional (2D) systems sheared at finite rates[16] revealed a broad distribution of rigid cluster sizes with increasing mean size as the jamming transition is approached, supporting a continuous rigidity transition, although becoming "sharper" as the shear rate is lowered. Similar results have been recently reported from analysis of sheared granular packings in experiments.[18] Following the observation that sheared frictionless packings acquire geometric characteristics associated with jamming,[20] the rigidity transition in such packings in 2D was analysed by including constraints associated with friction.[19] The size distribution of overconstrained clusters, similar to ref. 16, exhibits a broad distribution, supporting a continuous rigidity transition. In addition, the rigidity transition associated with jamming in frictional systems was studied in lattice models of

[a] *Theoretical Sciences Unit and School of Advanced Materials, Jawaharlal Nehru Centre for Advanced Scientific Research, Rachenahalli Lake Road, Bengaluru 560064, India. E-mail: varghese@jncasr.ac.in, sastry@jncasr.ac.in*
[b] *Department of Physics, Institute for Soft Matter Synthesis and Metrology, Georgetown University, Washington, DC, USA*
[c] *Department of Physics, Northeastern University, MA 02115, USA*

† Electronic supplementary information (ESI) available. See DOI: https://doi.org/10.1039/d3sm00725a

jamming where a continuous transition was observed except in a limiting case corresponding to infinite friction.[17]

These observations suggest that the nature of the rigidity transition could be an exception to the commonality of isotropic and shear jamming phenomenology outlined earlier. In this letter, we therefore investigate carefully the nature of the rigidity transition for both sheared frictional and frictionless packings, under both quasi-static and at finite shear rate. We find that the rigidity transition is unambiguously discontinuous under quasi-static shear. Such a transition appears rounded in the case of finite shear rate, but the dependence on shear rate clearly supports an approach to a discontinuous transition in the limit of vanishing shear rate.

1 Methods

In this section we discuss the models and methods used to obtain the shear jammed configurations in the frictional and frictionless case.

1.1 Frictionless shear jamming

It has previously been shown that the jamming density of a configuration of spheres under compression depends on the density of the initial equilibrated hard-sphere liquid[21,22] with denser hard-sphere liquids jamming at higher density. We denote ϕ_J as the minimum density at which isotropic jamming can be observed and ϕ_j as the variable jamming density with $\phi_j > \phi_J$. We use bidisperse soft-disk mixtures of size ratio 1 : 1.4 in this study. For this system, in 3D, $\phi_J \approx 0.648$ and the maximum ϕ_j observed in $\phi_j \approx 0.66$.[23] In 2D, $\phi_J \approx 0.84$; $\max\{\phi_j\} \approx 0.85$. Shear jammed frictionless packings are obtained by shearing unjammed soft-disks above ϕ_J as described in ref. 8 and 23–25. We equilibrate hard-disk configurations at high density ($\phi = 0.81$) using HOOMD,[26] which jam at a density $\phi_j > \phi_J$ with the protocol described in ref. 4. Unjammed configurations decompressed to a density ϕ, with $\phi_J < \phi < \phi_j$ undergoing shear jamming when subjected to athermal quasi-static shear (AQS). AQS is carried out by applying an affine transformation to the particle positions implementing the strain increment $\Delta\gamma$ followed by an energy minimization using conjugate gradient in LAMMPS.[27] We chose $\Delta\gamma = 5 \times 10^{-4}$ and stop the energy minimization when the total force acting on any particle is less than 10^{-13}. We study 3 independent samples of $N = 16\,384$ particles at a density of $\phi = 0.8485$.

1.2 Frictional shear jamming

Quasi-static shear simulations. We use the discrete element method (DEM)[28] to simulate frictional disks, using LAMMPS,[27] with linear and tangential spring dash-pot forces. The model includes damping in both normal and tangential directions, in addition to global viscous damping. The normal and tangential spring constants k_n and k_t are set to 2.0. The normal velocity damping η_n is set to 3.0 and the tangential damping η_t is set to $\frac{1}{2}\eta_n$. The global damping term η is also set to ≈ 3.

Shear is applied by performing an affine transformation of particle positions, with strain increments $\Delta\gamma$ followed by relaxation using DEM. Because of the damping terms, the system will eventually reach a force, torque balanced configuration if one waits long enough. Quasi-static shear requires reaching force/torque balance at each strain step. In practice, we consider the system to have reached force/torque balance when the total force (sum of total forces acting on the disks) is less than 10^{-11} or when the total kinetic energy of the system is less than 10^{-19}. The simulation is stopped when the number of timesteps reaches 2×10^9 regardless. The timescale required to relax the system diverges at the shear jamming transition as pointed out in ref. 29 and thus it is difficult to achieve force-balance close to the transition.

Finite rate simulations. We implement shearing at finite rates $\dot{\gamma}$ by performing DEM dynamics, after every strain step, for $\frac{\Delta\gamma}{\dot{\gamma}\mathrm{d}t}$ timesteps, where $\mathrm{d}t = 0.002$ is the timestep used in the DEM simulation.

We set $\Delta\gamma$ is 10^{-4} for finite rate shear and 10^{-3} for quasi-static shear. We perform finite rate shear on a system size of $N = 16\,384$ particles for 10 independent samples (and 20 samples for highest and lowest shear rate), and quasi-static shear with $N = 2000$ for 16 samples. The packing fraction ϕ of the system is 0.81. Further details of the simulations are described in the ESI,† Section I. We describe the results for friction coefficient $\mu = 1$ in the main text. Results with $\mu = 0.1$ can be found in the ESI,† Section V.

Definitions. The following quantities are used both in quasi-static frictionless and frictional simulations to identify the transition and to quantify the quality of force-balance achieved. $\left\langle \left| \vec{f}_{\mathrm{contact}} \right| \right\rangle$ is the average value of the contact force in a given configuration. This is defined as

$$\left\langle \left| \vec{f}_{\mathrm{contact}} \right| \right\rangle = \frac{\sum_{i=1}^{N_c} \left| \vec{f}_i^{\mathrm{contact}} \right|}{N_c}$$

where N_c is the total number of contacts in the system. $\left\langle \left| \vec{f}_{\mathrm{total}} \right| \right\rangle$ is the average of total force acting on each particle in the configuration. This is defined as

$$\left\langle \left| \vec{f}_{\mathrm{total}} \right| \right\rangle = \frac{\sum_{i=1}^{N} \left| \vec{f}_i^{\mathrm{total}} \right|}{N}$$

where $\vec{f}_i^{\mathrm{total}} = \sum_{j=1}^{N_{\mathrm{contacts}}^i} \vec{f}_{ij}^{\mathrm{contact}}$, with N_{contacts}^i being the number of contacts particle i has. In quasi-static simulations, $\left\langle \left| \vec{f}_{\mathrm{total}} \right| \right\rangle$ is expected to have a value close to zero in both jammed and unjammed configurations, as this is a measure of how good our force-balance is. With $\left\langle \left| \vec{f}_{\mathrm{total}} \right| \right\rangle$ being close to zero, if $\left\langle \left| \vec{f}_{\mathrm{contact}} \right| \right\rangle$ is non-zero then we can identify the configuration as being jammed.

We define rattlers as particles with less than the minimum number of contacts necessary for local rigidity, = 3 for frictionless, and 2 for frictional particles in 2D. For the rigidity analysis, we remove rattlers recursively from the system. The sizes of the system and rigid clusters reported in the results are after removing rattlers, unless specified otherwise.

1.3 Generalized isostaticity in frictional systems

A major distinction between frictionless and frictional jamming is the isostatic contact number Z at which jamming can occur in the absence of redundant constraints, which has been shown to range from $D + 1$ to $2D$ depending on the friction co-efficient μ[19,20,30,31] with $Z_{iso} = D + 1$ for $\mu = \infty$. This can be understood using the generalized isostaticity condition, obtained by considering additional conditions due to the "mobilized contacts".[30] The tangential frictional force between two particles has an upper bound due to the Coulomb threshold: $f_t \leq \mu f_n$ and the mobilized contacts are those for which $\frac{f_t}{f_n} \approx \mu$. n_m is defined as the number of mobilized contacts per particle, *i.e.* $n_m N$ is the total number of mobilized contacts. Considering a configuration with N particles and $n_m N$ mobilized contacts, the conditions that the contact network at jamming has to satisfy are DN force balance conditions, $\frac{D(D-1)}{2}N$ torque balance conditions and $n_m N$ Coulomb conditions. The number of constraints imposed by the contacts is $\frac{NDZ}{2}$ (since each contact constrains one translational and $D - 1$ rotational degrees of freedom). Z is by default computed excluding rattlers, and represented by Z_{NR} for clarity. Defining $Z_\mu = Z_{NR} - \frac{2n_m}{D}$, the generalized isostaticity condition is

$$Z_\mu^{iso} = Z_{NR} - \frac{2n_m}{D} = D + 1. \quad (1)$$

1.4 Rigidity analysis

For 2D networks arising in several contexts including jamming, the onset of rigidity has been analysed by employing the pebble game algorithm.[14] Each node of the network represents a disk in the present context and is assigned k pebbles ($k = 2$ for frictionless disks and $k = 3$ for frictional disks) representing the degrees of freedom. The constraints imposed by each contact are represented by 1 or 2 edges (2 for the frictional case, 1 for the frictionless case, as well as for a mobilised contact). A (k,l) pebble game ($l = 2$ indicates the global degrees of freedom) assigns pebbles recursively to edges, and based on such an assignment, decomposes the network into rigid clusters that are mutually floppy. Rigid clusters with redundant bonds (with no assigned pebbles) are termed over-constrained. A more detailed description of the algorithm is provided in ESI,† Section II. We employ the (3,2) pebble game to monitor the size of the largest rigid cluster in the system primarily, as well as the distribution of the size of rigid clusters. We have also verified that the character of the rigidity transition is not affected if we perform a (3,3) pebble game instead, considering the global degrees of freedom to be $l = 3$.

2 Results

2.1 Frictionless shear jamming

First, we discuss the results of the frictionless system, for which above jamming, energy minimization cannot remove all the overlaps in the system, resulting in finite contact forces. Note that the total force acting on each particle remains close to zero. As discussed in ref. 8 and 23, the configurations are isostatic ($N_c = (N - 1) \times 2$ after removing rattlers) at the jamming point. ($k = 2$, $l = 2$) pebble game analysis of isostatic configurations shows that the whole system is made up of a single rigid cluster, as shown in Fig. 1(b). Removing a single bond from this system leads to loss of rigidity, as shown in Fig. 1(a). The results of this analysis are summarized in Fig. 2. The shear jamming transition can be identified by the presence of finite contact forces (denoted by average contact force in the system $\left\langle \left| \vec{f}_{contact} \right| \right\rangle$) as well as by Z_{NR}. The average total force acting on the particles is denoted by $\left\langle \left| \vec{f}_{total} \right| \right\rangle$ and remains close to zero indicating that the particles are under force-balance. The rigidity transition occurs at the jamming transition point and is characterized by a discontinuous jump in the size of the largest cluster (orange curve in Fig. 2) where $N_{largest}$ is the size of the largest cluster and N is the size of the system – both computed after removing the rattlers. We note here that the pebble game can be used to identify rattlers. Also, our observation of discontinuous rigidity transition is unaffected by the presence of rattlers. However, the average coordination number at which transition occurs will be smaller than Z_{iso} if we keep the rattlers. This strongly discontinuous rigidity transition is also observed for isotropic jamming[10,16] and therefore a feature of frictionless jamming. This is in contrast with the continuous nature of rigidity transition in bond-diluted lattice models as discussed in ref. 10.

2.2 Finite rate shear of the frictional system

Next, we discuss the results from finite rate shear of frictional systems for shear rates $\dot{\gamma} = 5 \times 10^{-4}$, 5×10^{-5}, 5×10^{-6},

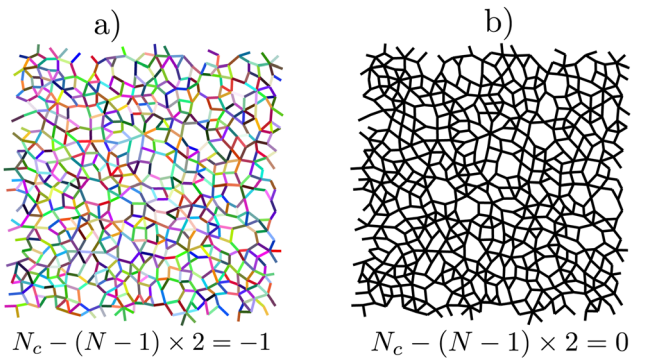

Fig. 1 Rigidity transition in sheared frictionless disk packings. Pebble game analysis on the isostatic networks yields a single rigid cluster consisting of the whole system. (b) Removal of one bond from that network results in a complete loss of rigidity, with the pebble game decomposing the system into multiple small rigid clusters. Bonds that are connected to each other and have the same color belong to the same cluster. A single bond is the smallest "cluster" in the system (a).

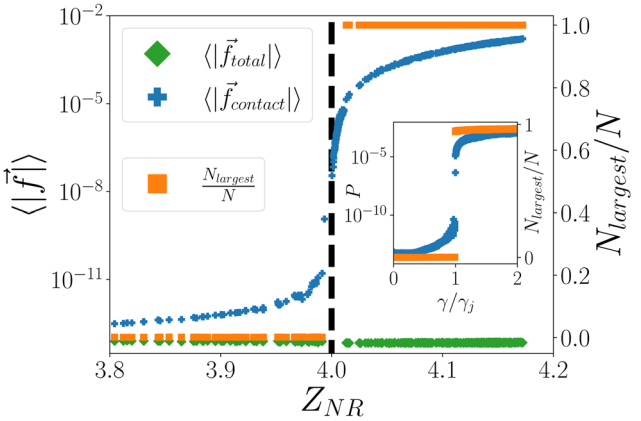

Fig. 2 Rigidity transition associated with shear jamming in frictionless systems. Rigidity transition can be seen as a discontinuous jump in the size of the largest cluster divided by the system size, both calculated after removing rattlers (orange). The transition occurs at the isostatic value of the non-rattler contact number, $Z_{NR} = 4$. This is also the point where the average contact force (blue) becomes non-zero, while the average total force on each particle (green) remains close to zero throughout. Inset shows pressure P (blue) *vs.* strain γ and the largest cluster size divided by the system size, both calculated after removing rattlers (orange). In the main graph and the inset, the y-axis on the right corresponds to the $\frac{N_{\text{largest}}}{N}$ data. Average total force, average contact force, and pressure correspond to the y-axis on the left.

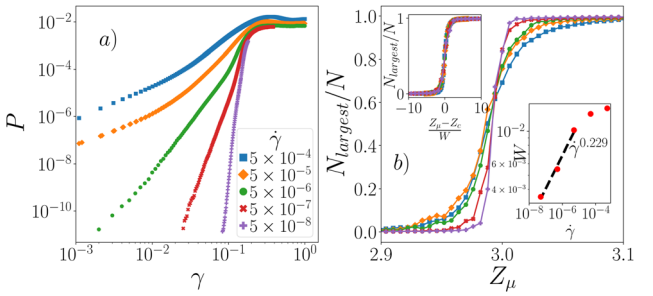

Fig. 3 Finite rate shear for $N = 16\,384$ with $\mu = 1$. (a) Pressure P *vs.* γ. (b) Fraction of the largest rigid cluster with the total number of particles (both quantities computed after removing rattlers) as a function of Z_μ. As $\dot{\gamma}$ is reduced, the transition becomes "sharper". Inset top left: Data from different shear rates collapse onto each other when scaled by the "width" W of the transition region. Inset lower right: The width of the transition region obtained by fitting the data. Dependence of W for the three smaller shear rates on $\dot{\gamma}$ can be described using a power-law suggesting that the transition becomes discontinuous as $\dot{\gamma} \to 0$.

5×10^{-7}, and 5×10^{-8}. The main observation from this set of simulations is that the rigidity transition associated with shear jamming becomes "sharper" as one reduces the shear rate, an observation also made in ref. 16. We have verified that the system is in the quasi-static regime with the inertial number $I = \frac{\dot{\gamma} d}{\sqrt{\frac{P}{\rho}}} < 10^{-3\,32}$ where d is the average diameter, P is the pressure and ρ is the density, for the smaller four $\dot{\gamma}$ except at very small strain values.

As shown in Fig. 3(a), the increase in pressure P with strain is noticeably sharper for smaller shear rates. To characterize the rigidity of these configurations we follow ref. 16, 18 and 19 and use the ($k = 3$, $l = 2$) pebble game on the contact network. Note that in the finite rate simulations, we do not simulate the system until it achieves force balance, and therefore for jammed as well as unjammed configurations, the net forces on the disks are finite. We use a threshold ε to identify mobilized contacts – if $\frac{|\vec{f}_t|}{|\vec{f}_n|} > \mu - \varepsilon$ then the contact is mobilized.[33] For simulations with $\mu = 1$, very few of our contacts are sliding and the choice of ε does not significantly affect the results presented. We choose $\varepsilon = 10^{-12}$ for the results in the main text. A discussion on the choice of ε is included in the ESI,† Section VI. Even though the system is not in force balance when sheared at a finite rate, we identify rattlers as particles with just one contact and remove them recursively. For the remaining contact network, we perform pebble game analysis and show in Fig. 3(b) the size of the largest rigid cluster as a function of the average contact number $Z_\mu = Z_{NR} - n_m$. The transition becomes sharper as one reduces $\dot{\gamma}$, and interestingly, the transition occurs at $Z_\mu \approx 3$, the isostatic value, for all shear rates. We fit the data using the logistic function $f(x) = \left[1 + e^{-\frac{x - Z_c}{W}}\right]^{-1}$ (as a reasonable but arbitrary choice) and use W as a measure of the width of the transition region. As the top left inset in Fig. 3(b) shows, the data can be collapsed using the fit values, with $Z_c \approx 2.99$. In the lower right inset, we show the behavior of W, whose dependence on $\dot{\gamma}$ can be described by a power law that implies that the transition becomes discontinuous at $\dot{\gamma} \to 0$. To our knowledge, this has not been reported for shear jamming transition.

Next, we study the rigid cluster size distribution as shown in Fig. 4 for the largest and the smallest $\dot{\gamma}$ studied. For both cases, we divide the region studied (in Z_μ) into three regimes – before the jamming transition, a regime covering the transition, and after the transition – and compute the distribution of the rigid cluster sizes separately for each of them. The distributions in the regime covering the transition are quantified by an exponent characterizing the power-law distribution of the rigid clusters. For $\dot{\gamma} = 5 \times 10^{-4}$, the exponent is -1.62 and for $\dot{\gamma} = 5 \times 10^{-8}$, the exponent is 2.17. While the transition in this regard appears continuous for both the shear rates studied, the distributions become progressively narrower as the shear rate decreases. The corresponding curves for the frictionless and frictional quasi-static shear show a faster than power law decay below the rigidity transition. We also calculate P_∞, the probability that a given disk belongs to a system spanning (percolating) rigid cluster, which is shown in the ESI,† Section IV. The P_∞ curves become progressively step-like with decreasing shear rate. Thus, we conclude that the appearance of a continuous transition is associated with the finite shear rates and absence of force/torque balance, rather than being an indication of the intrinsic nature of the shear jamming transition, or the presence of friction.

2.3 Quasi-static shear of frictional systems

To underscore our conclusions, we next consider quasi-static shearing of frictional disks, which is performed by applying an affine transformation and relaxing the system using DEM until the system reaches force balance. As noted before, the

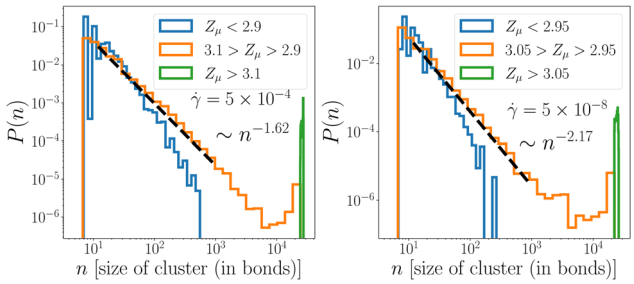

Fig. 4 Comparison of the rigid cluster size distribution between high and low $\dot{\gamma}$ studied. (a) $\dot{\gamma} = 5 \times 10^{-4}$ and (b) $\dot{\gamma} = 5 \times 10^{-8}$. Comparing the distribution of cluster sizes for the range covering 3, we see that $\dot{\gamma} = 5 \times 10^{-4}$ shows a broader distribution compared to the one at $\dot{\gamma} = 5 \times 10^{-8}$ as quantified by the exponent characterizing the power law distribution, indicating that the transition becomes discontinuous as the shear rate vanishes. The distribution corresponding to a given region in Z_μ is calculated by considering the sizes of all rigid clusters in a configuration with Z_μ in that region. Here we omit single bond clusters when distributions are calculated.

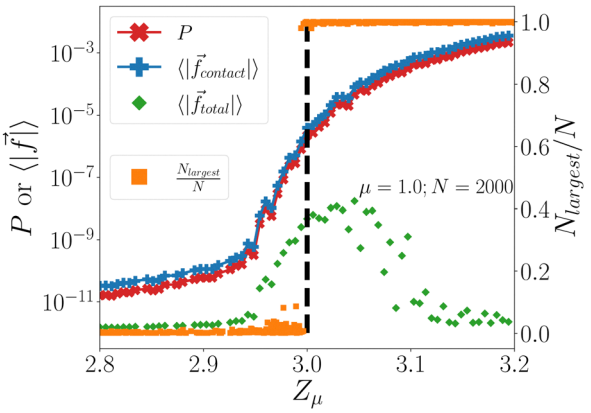

Fig. 5 Rigidity analysis of quasi-statically shear jammed frictional disks. The size of the largest rigid cluster in the system indicated by $\frac{N_{\text{largest}}}{N}$(orange) (calculated after removing rattlers) discontinuously jumps from nearly zero to one. The transition occurs as Z_μ crosses 3, the isostatic value. The contact forces (blue) and pressure (red) show a more gradual change, but the behavior of the net force on the disks reveals this to be a result of incomplete convergence, as indicated by the average of the net force of individual disks (green). Here, the y-axis on the right corresponds to the $\frac{N_{\text{largest}}}{N}$ data. Average total force, average contact force, and pressure correspond to the y-axis on the left.

relaxation near the jamming transition is very slow and therefore it is hard to generate force-balanced configurations near the jamming transition.[29,34] Given configurations that are fully relaxed, we define rattlers as particles that do not have finite forces acting on them. Disks with a single contact cannot sustain a non-zero force on that contact, which we remove recursively. In addition, given a friction co-efficient μ, disks with two contacts can be in force balance with finite forces only if the angle θ between the two contacts is large enough. If $\mu < \tan\left(\frac{\pi}{2} - \frac{\theta}{2}\right)$, these contacts cannot carry forces (see ESI,† Section III), and are thus also removed recursively. We note here that our result on the nature of the rigidity transition is not affected by the removal of rattlers.

These configurations are analyzed using the (k = 3, l = 2) pebble game, and the results are shown in Fig. 5. As Z_μ crosses the isostatic value 3, the largest rigid cluster encompasses the whole system, exhibiting a striking similarity with the behavior found for the frictionless case (Fig. 2). This observation is even more remarkable when one considers the behavior of the contact forces or pressure, *vs.* Z_μ, which show a more rounded change, as a result of the difficulty of converging to force balanced configurations, as indicated by the non-monotonic behavior of the net forces acting on the disks. P, $\left\langle \left| \vec{f}_{\text{contact}} \right| \right\rangle$ and $\left\langle \left| \vec{f}_{\text{total}} \right| \right\rangle$ shown are average values computed from all configurations having a given value of Z_μ. N_{largest}/N is a scatter plot from all trajectories.

Before closing, we briefly compare our results and conclusions with previous work mentioned earlier. While the conclusions in ref. 16 differ from ours, the sharpening of the rigidity transition has also been noted in ref. 16. In ref. 19, shear was applied to frictionless disk assemblies before friction was included in the rigidity analysis. While this procedure captures many features of sheared frictional disks, like the anisotropy and the emergence of a contact network that supports jamming in the presence of friction, subtle but important differences in the organization of contacts exist. Specifically, using the procedure of ref. 19, the fraction of redundant bonds rises continuously from below the isostatic contact number, as shown in the ESI,† Section VII, whereas they are strictly zero below the frictional jamming point. The absence of redundant bonds before the rigidity transition is a characteristic feature of jamming, as compared to rigidity percolation in spring networks and other systems.[15] Frictional rigidity transition studied on lattice models shows a continuous transition for a similar reason.[17] Bond-diluted lattice models do not ensure that the redundant bonds do not appear until the jamming point, unlike repulsive disk packings that reorganize the contact network such that there are no redundant bonds until the system reaches the jamming point. Our results differ from the analysis of experimentally sheared disk packings in ref. 18, for which we do not have a ready explanation, since the experimental protocol should be expected to closely agree with the quasi-static shear we employ, an inconsistency that needs to be further investigated.

3 Conclusions

In summary, our results unambiguously demonstrate that the rigidity transition associated with shear jamming in both frictionless and frictional disk packings is discontinuous in nature, when conditions of force and torque balance are met. Thus, the nature of the emergence of rigidity is the same for isotropic and shear jamming. Features that suggest a continuous transition are associated with partial relaxation of unbalanced forces, as our results for finite shear rate demonstrate, but such behavior approaches a discontinuous change as the

shear rate vanishes. Our results thus establish a key additional element in the shared phenomenology of isotropic and shear jamming.

Conflicts of interest

There are no conflicts to declare.

Acknowledgements

We thank S. Sarkar, S. Kumar, K. Daniels and S. Henkes for useful discussions. We acknowledge support from the Thematic Unit of Excellence on Computational Materials Science (TUE-CMS) and the National Supercomputing Mission facility (Param Yukti) at the Jawaharlal Nehru Centre for Advanced Scientific Research (JNCASR) for computational resources. D. B. acknowledges support from the National Science Foundation (grant no. DMR-2046683) and the Alfred P. Sloan Foundation. S. S. acknowledges support through the JC Bose Fellowship (grant no. JBR/2020/000015) from the Science and Engineering Research Board, Department of Science and Technology, India.

Notes and references

1 R. P. Behringer and B. Chakraborty, *Rep. Prog. Phys.*, 2018, **82**, 012601.
2 H. Zhang and H. Makse, *Phys. Rev. E: Stat., Nonlinear, Soft Matter Phys.*, 2005, **72**, 011301.
3 M. van Hecke, *J. Phys.: Condens. Matter*, 2009, **22**, 033101.
4 C. S. O'Hern, L. E. Silbert, A. J. Liu and S. R. Nagel, *Phys. Rev. E: Stat., Nonlinear, Soft Matter Phys.*, 2003, **68**, 011306.
5 P. Charbonneau, E. I. Corwin, G. Parisi and F. Zamponi, *Phys. Rev. Lett.*, 2015, **114**, 125504.
6 M. Wyart, *Phys. Rev. Lett.*, 2012, **109**, 125502.
7 E. Lerner, G. Düring and M. Wyart, *Soft Matter*, 2013, **9**, 8252–8263.
8 V. Babu and S. Sastry, *Phys. Rev. E*, 2022, **105**, L042901.
9 M. Baity-Jesi, C. P. Goodrich, A. J. Liu, S. R. Nagel and J. P. Sethna, *J. Stat. Phys.*, 2017, **167**, 735–748.
10 W. G. Ellenbroek, V. F. Hagh, A. Kumar, M. Thorpe and M. Van Hecke, *Phys. Rev. Lett.*, 2015, **114**, 135501.
11 J. Ortiz, E. Stanifer and X. Mao, arXiv, arXiv:2212.12129, 2022, preprint.
12 D. J. Koeze and B. P. Tighe, *Phys. Rev. Lett.*, 2018, **121**, 188002.
13 D. J. Koeze, L. Hong, A. Kumar and B. P. Tighe, *Phys. Rev. Res.*, 2020, **2**, 032047.
14 D. Jacobs and M. Thorpe, *Phys. Rev. E: Stat., Nonlinear, Soft Matter Phys.*, 1996, **53**, 3682.
15 M. Chubynsky, M.-A. Brière and N. Mousseau, *Phys. Rev. E: Stat., Nonlinear, Soft Matter Phys.*, 2006, **74**, 016116.
16 S. Henkes, D. A. Quint, Y. Fily and J. M. Schwarz, *Phys. Rev. Lett.*, 2016, **116**, 028301.
17 K. Liu, S. Henkes and J. Schwarz, *Phys. Rev. X*, 2019, **9**, 021006.
18 K. Liu, J. E. Kollmer, K. E. Daniels, J. Schwarz and S. Henkes, *Phys. Rev. Lett.*, 2021, **126**, 088002.
19 H. Vinutha and S. Sastry, *Phys. Rev. E*, 2019, **99**, 012123.
20 H. Vinutha and S. Sastry, *Nat. Phys.*, 2016, **12**, 578–583.
21 P. Chaudhuri, L. Berthier and S. Sastry, *Phys. Rev. Lett.*, 2010, **104**, 165701.
22 M. Ozawa, L. Berthier and D. Coslovich, *SciPost Phys.*, 2017, **3**, 027.
23 V. Babu, D. Pan, Y. Jin, B. Chakraborty and S. Sastry, *Soft Matter*, 2021, **17**, 3121–3127.
24 P. Das, H. Vinutha and S. Sastry, *Proc. Natl. Acad. Sci. U. S. A.*, 2020, **117**, 10203–10209.
25 N. Kumar and S. Luding, *Granular Matter*, 2016, **18**, 1–21.
26 J. A. Anderson, J. Glaser and S. C. Glotzer, *Comput. Mater. Sci.*, 2020, **173**, 109363.
27 S. Plimpton, *J. Comput. Phys.*, 1995, **117**, 1–19.
28 P. A. Cundall and O. D. Strack, *Geotechnique*, 1979, **29**, 47–65.
29 H. Vinutha, K. Ramola, B. Chakraborty and S. Sastry, *Granular Matter*, 2020, **22**, 1–8.
30 K. Shundyak, M. van Hecke and W. van Saarloos, *Phys. Rev. E*, 2007, **75**, 010301.
31 S. Henkes, M. van Hecke and W. van Saarloos, *EPL*, 2010, **90**, 14003.
32 GDR MiDi, *Eur. Phys. J. E: Soft Matter Biol. Phys.*, 2004, **14**, 341–365.
33 L. E. Silbert, *Soft Matter*, 2010, **6**, 2918–2924.
34 J. L. Shivers, S. Arzash, A. Sharma and F. C. MacKintosh, *Phys. Rev. Lett.*, 2019, **122**, 188003.

